Conducting and Characterizing Femto Flow Electrospray Ionization

Huishan Li,[a] Nicholas Allen,[a] Mengtian Li,[a] and Anyin Li[*a]*

[a] Department of Chemistry, University of New Hampshire, 23 Academic Way, Durham, NH 03824

[*]Corresponding authors: Anyin.Li@unh.edu

Abstract

Femto flow electrospray ionization (ESI) ranging from 240 fL/min to low pico flow (<10 pL/min) was conducted and measured using submicron emitter tip and relay ESI configuration. Signature analyte ion intensities and profiles were obtained. Obtained flow rate and ionization current enabled size calculation for initial charged nanodroplet.

Maintext

Electrospray ionization (ESI) is one widely used method in mass spectrometry[1] and surface modification[2]. The flow rate is a key parameter of ESI as it correlates with the size of the produced initial charged droplets.[3] Smaller initial charged droplets exhibit enhanced performances such as improved ionization efficiency, reduced nonspecific adduct, and lower sample consumption.[4-6] Reducing the flow rate for ESI is one continued research direction and the lower limits reported for micrometer emitter tips range 30–300 pL/min.[7-9]

Since the first introduction by Baker et al.,[4] submicron emitter tips have gained growing attention in ESI mass spectrometry. The smaller initial charged droplets produced by the submicron emitter tips effectively reduce nonspecific adducts and salt clusters,[10, 11] which is critical for the analysis of native biomolecules and complexes.[5, 12-14] However, except for the 26 pL/min for a 600 nm emitter tip,[15] the flow rates for most submicron emitter tips are unknown. Femtoamp electrospray ionization (fA ESI) was developed using both micrometer and submicron emitter tips.[16] The observed MS intensities, being 2–3 orders of magnitude lower than those produced by a 50 pL/min ESI,[17] suggest that the flow rates for these emitter tips could be in the femto range. These new findings bring challenges and exciting opportunities for the characterization and further development of low flow electrospray ionization.

Here we present the instrument methods for conducting and characterization of ultra-low ESI flow rates <10 pL/min. As shown in **Fig. 1**, a thin, long tapered submicron emitter tip was adopted to track volume change as small as 3 fL. Loading ca. 10 pL aqueous solution (**Fig. S1**) creates two air-liquid interfaces, one at the 100s nm tip opening and another at the backend with a ~10 μm diameter. These two interfaces had a combined evaporation rate of 10s pL/min under typical lab conditions. As evaporation is determined by the air-liquid interface (**Table S1** and **Fig. S2**), sealing the sample solution by hexane (**Fig. S1**) effectively reduced the evaporation to as low as 16 fL/min.

The relay ESI configuration[18] was adopted to trigger the ionization of ultra-low volume (<10 pL) sample solution without electrode contact, **Fig. 1a** and **Fig. S3**. Previously, it was demonstrated that ESI may be triggered by placing the electrode at a distance to the sample solution surface.[6, 19] This was attempted by placing a wire electrode in the hexane layer but no ionization was observed using voltages up to 4 kV, **Fig. S4**. This suggests that the hexane layer effectively prevented charge flow inside the emitter. In the case of

relay ESI, charge transport through the exterior space[9] was not interfered by the hexane layer. By using a wire-in submicron emitter tip as the primary source, adjustable flux (130 fA–2 nA)[16] of charge may be deposited onto the secondary emitter to trigger the ionization of the sample solution.

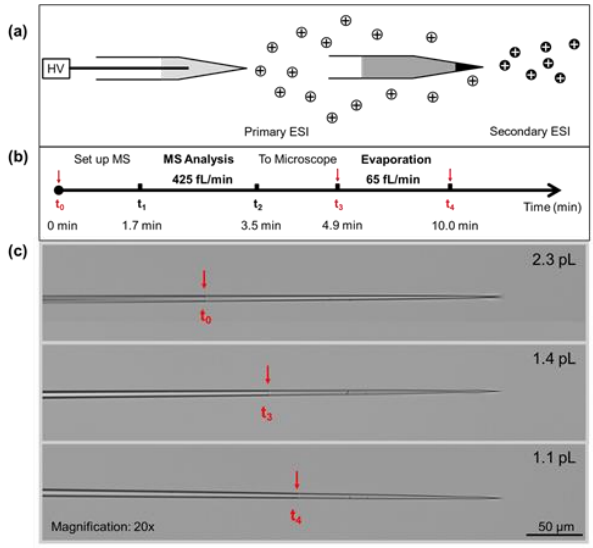

Figure 1. Conducting and measuring femto flow electrospray ionization mass spectrometry. **(a)** Scheme of the relay ESI setup. The sample solution (black) in secondary emitter was ionized by charges from the electrospray of the primary emitter (light grey). In the secondary emitter, a hexane layer (dark grey) reduced sample evaporation. **(b)** Timeline of a typical experiment that collects both mass spectra and flow rate data. **(c)** Microscope images of the emitter at three time points. Red arrows indicate the phase boundary between aqueous sample (right) and hexane (left).

Under continuously monitoring using optical microscopy, the consumption of the aqueous sample was indicated by the movement of hexane-water interface. Bright-field microscopy was effective in identifying interfaces as small as 1 µm, **Fig. S5**. Once the relay ESI was turned off, the solution consumption was due to evaporation via the tip opening. When the relay ESI was on, the ionization of sample solution was confirmed by the (>5 times) higher consumption rate than evaporation. **Video S1** shows one typical experiment in which the ESI flow rate and background evaporation were 450 fL/min and 37 fL/min, respectively. In the continuously recorded experiments, evaporation rates of 37, 180, 225, 55, 870 fL/min and ESI flow rates of 450, 980, 1100, 4000, 5980 fL/min were observed, as shown in **Video S1, S2**. There is a general correlation between the observed evaporation rates and ESI flow rates, **Fig. S6**. Both had a ~10-fold range, which is likely caused by the variation of emitter tips. In this work, the pulled submicron emitter tips had tip sizes ranging from 30–160 nm, **Table S2** and **Fig. S7**. Nevertheless, these femto and low pico flow rates are the lowest ESI flow rates reported in the literature.

The ionization at femto flow rates was further confirmed by mass spectrometry (MS). Volume measurements at multiple time points were carried out to obtain both ESI flow rates and corresponding mass spectra. **Fig. 1b, 1c** illustrate a typical experiment in which 1–10 pL aqueous sample was loaded into the emitter tip. A microscope image was taken at this time point (t_0) to measure the initial volume of the sample. From t_0 to t_1, the emitter was being mounted onto the relay ESI set up and aligned in front of the mass spectrometer. From t_1 to t_2, femto flow electrospray ionization was triggered, and the produced ions were analyzed by MS. From t_2 to t_3, the emitter was brought to the microscope to measure the sample volume. Lastly, another image was taken at t_4 to measure the evaporation rate under the lab conditions. Assuming the evaporation was constant during t_0–t_5, the electrospray flow rate was calculated by volume difference between V_0 (at t_0) and V_1 (at t_3) after subtracting the evaporation volumes from t_0 to t_1, and from

t_2 to t_3. In the experiments, the electrospray volumes were always >5 times larger than the estimated evaporation volumes. The obtained flow rate range is comparable to that obtained by continuous monitoring, **Table S3**. This suggests that the microscope lens (2 mm away) had no significant impact on the relay electrospray ionization.

As shown in **Fig. 2a**, an ESI flow rate of 425 fL/min produced an averaged intensity of 3.61E-1 for the analyte MRFA. Although this intensity is 5–6 orders of magnitude lower than that produced by a regular nanoESI, the clear isotope pattern of MRFA (**Fig. 2a** inset) indicates an adequate amount of analyte ions. The relative intensities of MRFA appeared to be low due to the higher intensities of the background signals ranging from m/z 100–350. These peaks were also observed when running the experiment using an empty secondary emitter tip, **Fig. S8**, suggesting that these peaks are more likely to be from the solution in the primary ion source, or desorbed from the glass surfaces. Slightly higher flow rates of 840 fL/min and 1057 fL/min produced higher MRFA intensity in the E1 range, **Fig. 2b, 2c**. For the above mass spectra, both TIC and EIC had continuous signals with intensity fluctuation within the same order of magnitude, **Fig. S9**.

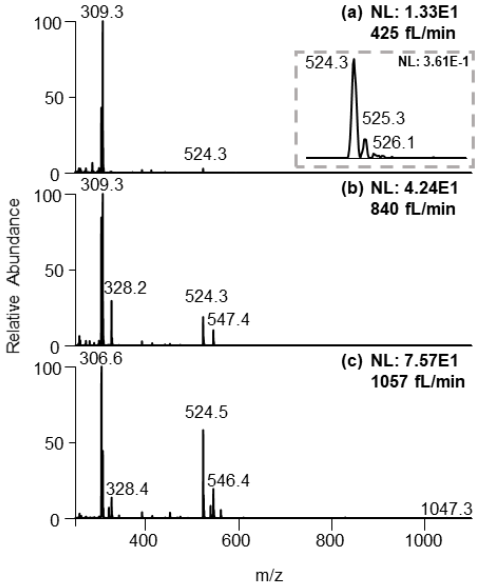

Figure 2. Full scan mass spectra of 100 μM MRFA at flow rates of **(a)** 425 fL/min, **(b)** 840 fL/min, and **(c)** 1057 fL/min.

On the LTQ-XL instrument, these femto to low pico flow ESI produced MS intensities (TIC flux intensities, ions per second) ranging from E2 to E4, positively correlated with flow rates. In comparison, a conventional nanoESI using the same sample solutions produced TIC intensities in the E6 to E7 range, **Fig. S9**. The >3 orders of magnitude difference in total ion current between nanoESI and femto flow ESI makes them easily distinguishable.

The current-voltage characteristics of the whole relay ESI set up were measured, **Fig. S10**. The onsets were typically at 100s fA and 300 V. At 1000 V, a total current of 218 pA was observed. Because the primary ions in relay ESI are diffusive and some of them may not be deposited onto the secondary emitter, the actual ionization current of the sample solution is lower than the total current, i.e., <218 pA. Ionization current ($\boldsymbol{I_{obs}}$) and flow rate ($\boldsymbol{V_f}$) allow the calculation of the average size for the initial charged droplets. Assume each initial charge droplet is at 70% Rayleigh limit, and imagine $\boldsymbol{t}$ is the average ejection time for each initial charged droplet, we have

$$I_{obs} \cdot t = 0.7 \cdot Z_r = 0.7 \cdot 8\pi\sqrt{\varepsilon_0 \gamma R_i^3} \quad (1)$$

to describe the observed ionization current I_{obs} and the charge on each droplet. Where Z_r is the charge on the droplet, R_i is the droplet radius, ε_0 is the permittivity, and γ is the surface tension of the droplet.[20] Similarly,

$$V_f \cdot t = V_d = \frac{4}{3}\pi R_i^3 \quad (2)$$

describes the flow rate (V_f) and the volume (V_d) of each droplet. Divide the first equation by the second, and solve for R_i, the following equation is obtained for the droplet radius:

$$R_i = \sqrt[3]{\frac{(0.7 \times 6)^2 \varepsilon_0 \gamma \cdot V_f^2}{I_{obs}^2}} \quad (3)$$

Recently, Bush et al. reported <10 nL/min flow rate and 30 nA ionization current in a nanoESI experiment.[21] Plug in the flow rate and current, equation (3) returns a diameter of <140 nm, which is in line with the measured size of 60 nm. In this work, the measured flow rate of 425 fL/min and a <218 pA ionization current indicates that the initial charged droplets are on average no smaller than 5 nm, which is on par with the estimated droplet size for submicron emitter tips.[13]

Operating submicron emitter tips are known to have practical problems in loading and spraying. One work reported 70% success rate for sample loading from the back end.[12] Clogging during electrospray is another common problem. In this work, front-loading through the emitter tip effectively filters out particles larger than the tip opening, which could reduce the chance of clogging. Yet, clogging events were still observed to cause the sudden disappearance of the analyte ion signal. Interestingly, solvent evaporation was not blocked after the clogging, suggesting that the tip was partially clogged and filtered out the analytes, **Fig. S11**. When running a protein-peptide mixture solution (MRFA and cytochrome c), similar partial clogging was sometimes observed, eliminating ion signal of the larger analyte, i.e., cyt c, **Fig. S12**.

When using emitter tips that produced higher flow rates in low the pico flow (1–10 pL/min) range, cyt c signal was readily observed. As shown in **Fig. 3a**, a flow rate of 7.7 pL/min produced a 4.8E2 signal intensity for the cyt c peaks. The intensity is analogous to that of the wire-in ESI using a similar submicron emitter tip (**Fig. 3b**) and is two orders of magnitude lower than that of nanoESI using micrometer emitter tip (**Fig. 3c**). In comparison, the flow rate is more than three orders of magnitude lower than that of a typical nanoESI.[9, 21] This confirms the improved overall ionization and transmission efficiency at lower flow, which aligns with previous observation with lower current ion beams.[16]

Interestingly, the ion intensity produced by fA ESI[16] (**Fig. 3d**) is two orders of magnitude lower than that produced by this 7.7 pL/min relay ESI. Assuming the overall ionization and transmission efficiency to be similar or slightly enhanced for this lower ion current, the flow rate for fA ESI is likely to be higher than 77 fL/min. Plug in this and the 400 fA ionization current,[16] equation (3) returns a size of >21 nm for the fA ESI. Considering that the hydrodynamic radius in cyt c is 1.7 ±0.2 nm,[22, 23] the calculated droplet size confirms the generation of charged droplets in fA ESI and rules out the possible hypothesis[24] of direct ion emission[25] from a nanoscale meniscus in the emitter tip, which would be similar to the electrohydrodynamic atomization[26] in vacuum.

The charged droplets produced by these low flow ESI methods were evaluated using the charge state pattern of cyt c. The protein solution was prepared without any buffering agent to reveal the altered chemical environments. The submicron emitter tip (both relay ESI and wire-in ESI) produced higher average charge states (7.5 and 7.1), **Fig. 3a, b**. It is worth noting that these higher charge states are all among the 7+, 8+ folded charge states. The trend of producing more of the higher charged native states when using smaller emitter tip (or channel) aligns with previous reports.[4, 27] The combination of relay ESI and submicron emitter has pushed this trend to an extreme. The highly abundant 8+ peak and the lack of 9+, 10+ peaks produced an oddly asymmetrical pattern that obviously deviates from the typical Gaussian profile patterns produced by ESI. In comparison, a submicron emitter in the wire-in mode produced symmetrical profiles, **Fig. 3b**. Symmetrical Gaussian-like profile of protein ions is believed to be the result of solution phase pH equilibria.[28] the disappearance of such symmetry suggests potential gas phase processes are at play. Native cyt c protein has a calculated Rayleigh limit of 8.6.[29] Lower average charge states (ACS 6.8–7.2) were produced due to the loss of charge carrier by ion emission at a threshold lower than the Rayleigh limit, as described in the combined charge residue and field emission model.[30] The ACS of 7.5 in **Fig. 3a** with only native peaks indicates that a significant population of the charged droplets has surpassed the threshold for charge carried emission. In relay ESI,[18] the primary charge not deposited onto the secondary emitter may coexist with the ESI plume. These surrounding extra charges could have suppressed the emission of charge carrier in the late stage of the ESI droplet, thus squeezing peaks into a narrower distribution of higher charge states, which could enhance the sensitivity for low concentration samples.

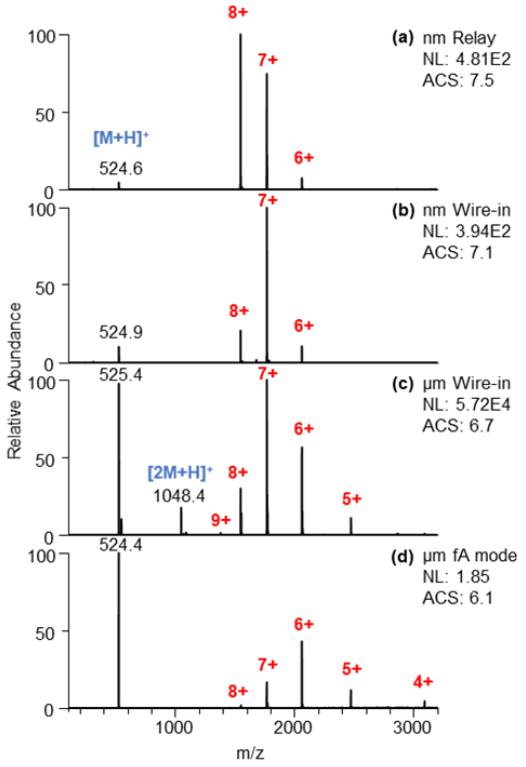

Figure 3. Full scan mass spectra of 50 µM cyt c and 50 µM MRFA aqueous mixture under different conditions. **(a)** relay ESI using submicron emitter tip with a 7.7 pL/min flow rate. **(b)** wire-in ESI using submicron emitter tip **(c)** nanoESI using micrometerr emitter tip. **(d)** fA ESI using micrometer emitter tip.

In comparison, nanoESI (**Fig. 3c**) produced an ACS of 6.7 with a symmetrical profile that also contains the partially unfolded 9+ charge states.[31, 32] When higher voltage was applied, higher average charged states and increasing abundances of partially unfolded protein ions (9+, 10+) were observed, **Fig. S13**. A similar

trend was observed when using submicron emitter using wire-in configuration, **Fig. S14.** The unfolding indicates significant pH evolution of the unbuffered charged droplets. For fA ESI, even lower native charge states (ACS 6.1) suggests a charge-reducing[33] effect, **Fig. 3d**.

Comparing the relative ion intensities of protein and MRFA, the submicron emitter tips (**Fig. 3a, 3b**) produced similarly high ratios 36:1 and 13:1 that favor the cyt c protein. NanoESI (**Fig. 3c**) produced a less high relative ratio (1.5:1). The fA ESI produced a ratio (0.77:1) that is closest to the actual concentration ratio (**Fig. 3d**). These results indicate that the relative ionization efficiency is very sensitive to experimental parameters, including flow rate, ionization current, and emitter tip size.

The ionization of other classes of analytes was also measured, **Table S3**. For some of them, the ESI flow rate may be calculated using the loaded sample volume and sample depletion time as indicated by MS. For example, a glycan mixture solution of 6.35 pL was consumed in 2.27 minutes by relay ESI, corresponding to a consumption flow rate of 2.8 pL/min, **Fig. S15**. The same emitter recorded a comparable flow rate of 4.5 pL/min when using the more complicated workflow (**Fig. 1b)**. However, this simplified depletion time approach may not be applied for those analytes which may adhere to the emitter tip to produce similar signal intensity after the depletion of sample solution, as can be seen in the cases of amitriptyline and acetylcholine, **Fig. S16**.

In summary, femto to low pico flow rates electrospray ionization were measured for the first time. Compared with nanoESI, femto flow ESI exhibits >2 orders of magnitude lower ion flux intensities, <218 pA ionization current, and >3 orders of magnitude lower low flow rates. These characteristics could serve as indicators for femto flow ionization in experiments when flow rate measurement is not available. The femto flow enabled the use of highly concentrated sample solutions in the experiments. In a typical experiment, 10s attomole per MS scan produced signal intensity above the detection limit. This absolute sensitivity is on par with conventional ESI and indicates excellent ionization efficiency in femto ESI. For a non-buffered protein solution, the low flow ionization modes allow native charge states to be produced in either charge-enhancing or charge-reducing manners. The measured flow rate and ionization current enable the calculation of the size of initial charged nanodroplets.

There are no conflicts to declare.

Notes and References

1. J. B. Fenn, M. Mann, C. K. Meng, S. F. Wong and C. M. Whitehouse, *Science*, 1989, **246**, 64-71.

2. S. Rauschenbach, F. L. Stadler, E. Lunedei, N. Malinowski, S. Koltsov, G. Costantini and K. Kern, *Small*, 2006, **2**, 540-547.

3. L. deJuan and J. F. delaMora, *J. Colloid Interface Sci.*, 1997, **186**, 280-293.

4. E. M. Yuill, N. Sa, S. J. Ray, G. M. Hieftje and L. A. Baker, *Anal. Chem.*, 2013, **85**, 8498-8502.

5. T. Kenderdine, Z. Xia, E. R. Williams and D. Fabris, *Anal. Chem.*, 2018, **90**, 13541-13548.

6. Z. Wei, X. Xiong, C. Guo, X. Si, Y. Zhao, M. He, C. Yang, W. Xu, F. Tang, X. Fang, S. Zhang and X. Zhang, *Anal. Chem.*, 2015, **87**, 11242-11248.

7. I. Marginean, K. Tang, R. D. Smith and R. T. Kelly, *J. Am. Soc. Mass. Spectrom.*, 2014, **25**, 30-36.

8. G. Huang, G. Li and R. G. Cooks, *Angew. Chem. Int. Ed.*, 2011, **50**, 9907-9910.

9. M. Li, H. Li, N. R. Allen, T. Wang, L. Li, J. Schwartz and A. Li, *Chemical Science*, 2021, **12**, 1907-1914.

10. A. C. Susa, Z. Xia and E. R. Williams, *Anal. Chem.*, 2017, **89**, 3116-3122.

11. Z. Xia and E. R. Williams, *J. Am. Soc. Mass. Spectrom.*, 2018, **29**, 194-202.

12. G. T. H. Nguyen, T. N. Tran, M. N. Podgorski, S. G. Bell, C. T. Supuran and W. A. Donald, *ACS Cent Sci*, 2019, **5**, 308-318.

13. E. G. B. Bolivar, D. T. Bui, E. N. Kitova, L. Han, R. X. B. Zheng, E. J. Luber, S. Y. Sayed, L. K. Mahal and J. S. Klassen, *Anal. Chem.*, 2021, **93**, 4231-4239.

14. E. M. Panczyk, J. D. Gilbert, G. S. Jagdale, A. Q. Stiving, L. A. Baker and V. H. Wysocki, *Anal. Chem.*, 2020, **92**, 2460-2467.

15. J. Hu, X. X. Jiang, J. Wang, Q. Y. Guan, P. K. Zhang, J. J. Xu and H. Y. Chen, *Anal. Chem.*, 2016, **88**, 7245-7251.

16. N. R. Allen, H. Li, A. Cheung, G. Xu, Y. Zi and A. Li, *Int. J. Mass spectrom.*, 2021, **469**, 116696.

17. M. Li, H. Li, N. R. Allen, T. Wang, L. Li, J. Schwartz and A. Li, *Chemical Science*, 2020.

18. A. Li, A. Hollerbach, Q. Luo and R. G. Cooks, *Angew. Chem. Int. Ed.*, 2015, **54**, 6893-6895.

19. A. J. Schwartz, J. T. Shelley, C. L. Walton, K. L. Williams and G. M. Hieftje, *Chemical science*, 2016, **7**, 6440-6449.

20. L. Rayleigh, *The London, Edinburgh, and Dublin Philosophical Magazine and Journal of Science*, 1882, **14**, 184-186.

21. K. L. Davidson, D. R. Oberreit, C. J. Hogan and M. F. Bush, *Int. J. Mass spectrom.*, 2017, **420**, 35-42.

22. C. Ghosh, M. A. AMIN, B. Jana and K. Bhattacharyya, *Journal of Chemical Sciences*, 2017, **129**, 841-847.

23. E. Aliyari and L. Konermann, *Anal. Chem.*, 2021, **93**, 12748-12757.

24. L. A. Baker and G. S. Jagdale, *Curr. Opin. Electrochem.*, 2019, **13**, 140-146.

25. B. A. Thomson and J. V. Iribarne, *J. Chem. Phys.*, 1979, **71**, 4451-4463.

26. D. P. H. Smith, *IEEE Trans. Ind. Appl.*, 1986, **22**, 527-535.

27. Y. Li and R. B. Cole, *Anal. Chem.*, 2003, **75**, 5739-5746.

28. R. Guevremont, K. W. M. Siu, J. C. Y. Leblanc and S. S. Berman, *J. Am. Soc. Mass. Spectrom.*, 1992, **3**, 216-224.

29. S. J. Allen, A. M. Schwartz and M. F. Bush, *Anal. Chem.*, 2013, **85**, 12055-12061.

30. C. J. Hogan, Jr., J. A. Carroll, H. W. Rohrs, P. Biswas and M. L. Gross, *Anal. Chem.*, 2009, **81**, 369-377.

31. J. K. Lee, S. Kim, H. G. Nam and R. N. Zare, *Proc. Natl. Acad. Sci. U.S.A.*, 2015, **112**, 3898-3903.

32. J. C. May, E. Jurneczko, S. M. Stow, I. Kratochvil, S. Kalkhof and J. A. McLean, *Int. J. Mass spectrom.*, 2018, **427**, 79-90.

33. A. Q. Stiving, B. J. Jones, J. Ujma, K. Giles and V. H. Wysocki, *Anal. Chem.*, 2020, **92**, 4475-4483.